AGU PUBLICATIONS

JGR

Journal of Geophysical Research: Oceans

RESEARCH ARTICLE

10.1002/2014JC010141

A weather-type statistical downscaling framework for ocean wave climate

Paula Camus[1], Melisa Menéndez[1], Fernando J. Méndez[1], Cristina Izaguirre[1], Antonio Espejo[1], Verónica Cánovas[1], Jorge Pérez[1], Ana Rueda[1], Inigo J. Losada[1], and Raúl Medina[1]

[1]Environmental Hydraulics Institute "IH Cantabria," Universidad de Cantabria, Cantabria, Spain

Key Points:
- A weather-type approach to statistically downscale multivariate wave climate
- The interannual variability of monthly sea-state parameters is reproduced
- A useful tool to analyze wave climate at different time scales

Correspondence to:
F. J. Méndez,
mendezf@unican.es

Citation:
Camus, P., M. Menéndez, F. J. Méndez, C. Izaguirre, A. Espejo, V. Cánovas, J. Pérez, A. Rueda, I. J. Losada, and R. Medina (2014), A weather-type statistical downscaling framework for ocean wave climate, *J. Geophys. Res. Oceans*, *119*, doi:10.1002/2014JC010141.

Received 12 MAY 2014
Accepted 17 SEP 2014
Accepted article online 22 SEP 2014

Abstract Wave climate characterization at different time scales (long-term historical periods, seasonal prediction, and future projections) is required for a broad number of marine activities. Wave reanalysis databases have become a valuable source of information covering time periods of decades. A weather-type approach is proposed to statistically downscale multivariate wave climate over different time scales from the reanalysis long-term period. The model calibration is performed using historical data of predictor (sea level pressure) and predictand (sea-state parameters) from reanalysis databases. The storm activity responsible for the predominant swell composition of the local wave climate is included in the predictor definition. *N*-days sea level pressure fields are used as predictor. *K*-means algorithm with a postorganization in a bidimensional lattice is used to obtain weather patterns. Multivariate hourly sea states are associated with each pattern. The model is applied at two locations on the east coast of the North Atlantic Ocean. The validation proves the model skill to reproduce the seasonal and interannual variability of monthly sea-state parameters. Moreover, the projection of wave climate onto weather types provides a multivariate wave climate characterization with a physically interpretable linkage with atmospheric forcings. The statistical model is applied to reconstruct wave climate in the last twentieth century, to hindcast the last winter, and to project wave climate under climate change scenarios. The statistical approach has been demonstrated to be a useful tool to analyze wave climate at different time scales.

1. Introduction

Accurate characterization of local wave climate is required in series of sectors such as shipping, offshore industry, marine engineering, and coastal management. Wave climate variability plays a significant role in numerous geophysical processes. Operations of marine carriers, logistics of marine structures, coastal erosion, or flooding risk are some examples where multivariate behavior of waves is essential. Wave climate is traditionally characterized from two sources: observations (buoys, satellites, and voluntary observing ship (VOS) data) and outcomes from numerical models (dynamical downscaling). Buoys provide the most reliable data; however, their records are usually not longer than 20 years, have notable gaps, and are very scattered at sea. Satellite observations present a global coverage, but this source of data is only available since 1992 with a nonregular time resolution. VOS data provide the longest records of independent sea and swell parameters [*Gulev and Grigorieva*, 2006] and reliable climate variability and trends with less inhomogeneities than wave hindcast [*Gulev et al*., 2003]. However, their sampling is insufficient and they require correction algorithms. The dynamical downscaling outputs are a good alternative to observations, but they require a high-quality bathymetry and wind fields and are computationally expensive.

When atmospheric data are available, an alternative to dynamical downscaling is the statistical downscaling. The statistical downscaling (SD) method typically adopts a "perfect prognosis" approach, in which high-resolution simulations of the variables of interest are based on real-world statistical relationships between large-scale atmospheric predictors and a local-scale predictand. The main advantage of the statistical approach is that it is computationally inexpensive; therefore, it is suitable for a faster predictand characterization, to get long-term simulations, or to develop multiple realizations from different forcing conditions (i.e., outputs from climate change scenarios). Some assumptions are inherent in the perfect prognosis downscaling approach: (i) variability of the local variable should be explained by the statistical connection, (ii) changes in the mean climate should lie within the range of its natural variability, and (iii) the relationships should be stationary. Long observation time series, physical explanation of the relation between the

large-scale predictor and the local predictand, and reliable predictor simulations by Global Circulation Models (GCMs) fulfill these conditions [*Wilby et al*., 2004].

Different approaches can be applied to develop a SD model. *Giorgi et al*. [2001] classified the methods into: (i) transfer functions, (ii) weather-type approaches, and (iii) stochastic weather generators. The performance of the SD techniques can be found in a high number of works for different regions using a broad range of predictands. For example, *Gutiérrez et al*. [2013] compare the performances of different SD methods (from the analog, weather typing, and regression families) for downscaling temperatures in Spain. Each method has its own strengths and weaknesses, reproducing certain local weather statistical characteristics with more or less accuracy, being difficult to select one against the other, always depending on each particular case. Other relevant aspects which determine the skill of the SD method are the predictor choice, regarding variables and the spatial domain [*Fowler et al*., 2007]. In the case of sea surface waves, sea level pressure (SLP) fields and the squared SLP gradient fields have demonstrated to be good predictors [*Wang et al*., 2012; *Casas-Prat et al*., 2014]. This is especially relevant for applications of climate projections, since the SLP variable is supposed to be less biased than wind fields from GCMs [*Caires et al*., 2006].

The SD applications to analyze wave climate are usually limited to climate projections of the significant wave height (H_s), a parameter of the sea state. Most of the developed works are based on multivariate linear regression models between the SLP predictor and the H_s at seasonal or hourly scale [*Wang et al*., 2012; *Wang and Swail*, 2006; *Wang et al*., 2004; *Casas-Prat et al*., 2014] or extreme models, modeling the interannual variability using covariates defined by the SLP predictors [*Wang et al*., 2004; *Wang and Swail*, 2006; *Caires et al*., 2006; *Izaguirre et al*., 2010]. However, H_s is not the only variable of concern to deal with wave climate processes. Other sea-state parameters (e.g., peak period and mean wave direction) are required to analyze climate change effects in coastal structures [*Suh et al*., 2012] or wave energy resources [*Hemer et al*., 2010]. For example, wave direction is particularly critical for calculating littoral drift and associated estimates of sand budgets to determine coastal erosion.

In this work, an SD framework based on weather types is presented. Statistical models find difficult to reproduce waves in swell-dominated areas [*Hemer et al*., 2012]. To overcome this problem, the recent history of atmospheric conditions responsible for the swell component in the study area is going to be introduced in the predictor definition. A statistical relationship between the weather types and the whole probability distribution of multivariate local wave climate is established. The SD model is applied in two locations in the North Atlantic Ocean, in the Irish and the Spanish coasts. For these locations, the SD model is validated and some applications are shown: a local wave climate characterization, a long-term historical reconstruction, an update of a wave hindcast database, and the simulation of wave climate projections.

The paper is structured as follows. Section 2 presents the statistical downscaling framework proposed. Section 3 shows the application of the method to a particular case study. This section includes the definition of the predictor and predictand, the application of the weather classification technique, the description of the relationship between the synoptic patterns and the local wave climate, and the results of the validation period. Section 4 presents several applications of the statistical downscaling method including the characterization, hindcast, and projection of wave climate. Section 5 contains the summary and conclusions.

2. The Statistical Downscaling Method

Regarding wave climate, the aim of a statistical downscaling method is to estimate local waves (predictand) from global atmospheric conditions (predictor), based on a statistical relation. A weather typing method is proposed in this study. The flowchart summarizing the statistical method is shown in Figure 1. The steps of the methodology are: (1) collection of historical data for the predictor and predictand; (2) definition of the predictor at daily scale; (3) classification of predictor conditions in a reduced number of weather types; (4) establishing the relationship between predictor and predictand; (5) validation of the statistical model.

First, historical data of both atmospheric predictor and wave climate predictand are required to define the statistical model between predictand and predictor.

Regarding the predictor definition on a daily scale, the variables are the SLP and the squared SLP gradients. The spatial domain and temporal coverage of the predictor should be specified for each location where waves are downscaled. Spatial domain should cover the oceanic basin area of wave generation reaching that particular location. Recent historical atmospheric conditions should be included in the predictor in

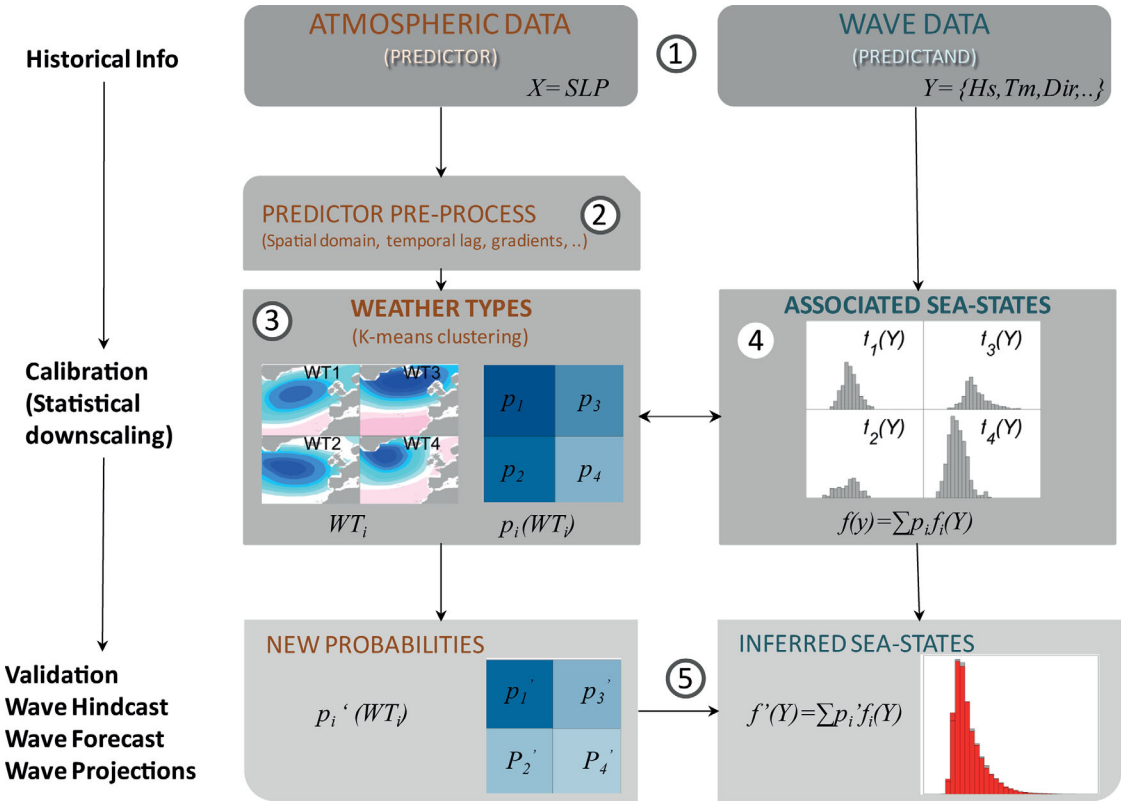

Figure 1. Flowchart representing the statistical downscaling methodology.

order to take into account the generation and propagation processes of the waves reaching a specific location.

In the third step, the SLP predictor database is partitioned into a certain number of clusters, named weather types (WTs), applying a classification technique. Each WT represents a synoptic atmospheric circulation pattern.

WT classification is obtained combining three data mining techniques: first, a principal component analysis (PCA) is applied to the predictor variable in order to reduce the data dimensionality and simplify the classification process. Second, the predictor in the EOFs space is clustered using *k*-means algorithm (KMA). Finally, the set of WTs is organized using a similarity criterion.

PCA projects the original data on a new space searching for the maximum variance of the sample data. The eigenvectors (empirical orthogonal functions, EOFs) of the data covariance matrix define the vectors of the new space. The original data projections over the new vectors are the Principal Components (PCs). The EOFs are ranked in increasing order of explained variance. Therefore, a smaller number of PCs than the original data dimension is considered, keeping a high amount of variance. The KMA divides the data space into a number of clusters, each one defined by a prototype and formed by the data for which the prototype is the closest [*Hastie et al*., 2001]. The maximum-dissimilarity algorithm (MDA) is applied to initiate the prototypes, which guarantees a deterministic classification and the most representative initial subset.

The clusters are organized in a bidimensional lattice, which allows an intuitive visualization of the classification. The algorithm, based on a similarity criterion, starts locating the clusters into a bidimensional lattice. The distance between each cluster WTi and its closest neighbors in the lattice are calculated. Permutations of the cluster locations in the lattice are performed, calculating the sum of the distances in each permutation. The best organized lattice is the one with the minimum sum of distance [*Bermejo and Ancell*, 2009]. Results are almost similar to the selforganizing maps due to the fact that similar patterns in the original space are close in the lattice, with the advantage of a better exploration of the data space, strengthened by an MDA initialization [*Camus et al*., 2011].

The fourth step consists of defining the statistical relationship between the predictor and predictand. The predictand is defined as the sea-state parameters at the location of interest. The sea states are associated with each cluster (hourly sea states during each daily predictor field represented by the corresponding cluster), allowing a nonlinear relationship. The probability distributions of different variables $f_i(y)$, such as the univariate distribution of the H_s parameter or the joint distribution of H_s and mean period (T_m), are calculated for each WT_i. This statistical relation is established for a calibration period. Although in the state of the art the statistical downscaling methods are sometimes calibrated separately for each season, in our approach, the classification process is performed for the whole calibration period due to the fact that future seasonal climates might not exactly correspond to the present ones [*Maraun et al*., 2010].

Hence, the marginal and joint distributions (empirical probability density functions) of the sea-state parameters and any derived statistic can be estimated for the whole calibration time period as follows:

$$f(y)=\sum_{i=1}^{M} p_i \cdot f_i(y), \tag{1}$$

where p_i is the probability of WT_i. The probability of occurrence (p_i) of a WT_i is estimated from the number of daily atmospheric predictor situations represented by each WT_i, so that $\sum_{i=1}^{M} p_i = 1$, where M is the number of weather types.

The estimation of the sea-state parameters for a time period outside the calibration period is based on the new probabilities of the WTs from the SLP predictor. The sea-state distributions for a new time period can be estimated as:

$$f'(y)=\sum_{i=1}^{M} p_i' \cdot f_i(y), \tag{2}$$

being p'_i the probability of WTs for the new time period.

The final step of the definition of the statistical downscaling model is the validation. Monthly sea-state parameters are calculated based on the distribution of sea states associated with each WTi and the probabilities of the WTs for the validation period.

3. Case Study

The SD model is applied in the North Atlantic region at two locations by establishing a statistical relationship between large-scale atmospheric circulation patterns and the probability distributions of several parameters of the sea states.

3.1. Data

3.1.1. Predictor

The global SLP fields of the NCEP/NCAR reanalysis-I [*Kalnay et al*., 1996], from the National Center for Environmental Prediction-National Center for Atmospheric Research, are used as the predictor in the SD model. This atmospheric reanalysis spans from 1948 to present. Multiple instrumental measurements were integrated in an assimilation process. Inhomogeneities were found to be caused by changes in the observing system. NCEP/NCAR reanalysis is less reliable during the earliest decade (1948–1957), due to fewer upper-air data observations [*Kistler et al*., 2001]. After 1957, data coverage in the North Hemisphere was large enough to effectively constrain the model and avoid large inhomogeneities. However, homogeneity in the Southern Hemisphere can only be assumed after 1980 due to low data coverage [*Sterl*, 2004]. Therefore, data from 1960 to 2013 are used in this work. The used SLP data from NCEP-NCAR reanalysis-I consist of 6 hourly fields on a 2.5° by 2.5° long-lat global grid.

3.1.2. Predictand

Historical data of the local wave climate predictand are required in the SD model. The historical wave information used in this work is the ocean wave reanalysis database Global Ocean Waves (GOW) [*Reguero et al*., 2012]. GOW has been generated with the third generation model WaveWatch III, which solves the spectral action density balance equation for wave number direction spectra using finite differences [*Tolman*, 2009]. GOW encompasses several spatial domains, a global grid with a spatial resolution of 1.5° by 1°, forced by

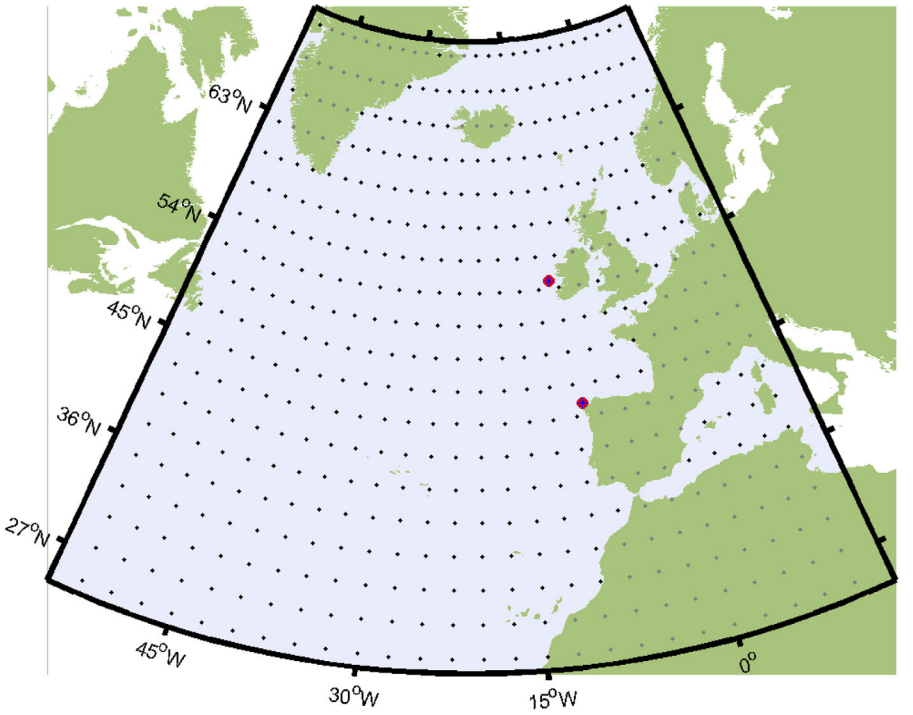

Figure 2. Selected spatial domain of SLP predictor (only black grid points are considered). Red circles show the locations of the analyzed predictand (local wave climate).

the 6 hourly wind fields of NCEP-NCAR reanalysis-I (more details in *Reguero et al*. [2012]) and several nested regional domains around (e.g., Pacific and Atlantic American regions described in *Izaguirre et al*. [2013]). Here we use waves from a GOW regional simulation over the European Atlantic area. The regional spatial domain spans from 27.25°N to 57.25°N and 20°W to 37°E, with a resolution of 0.25°. The European Atlantic domain is forced with wind fields from SeaWind I, a dynamic atmospheric downscaling from NCEP-NCAR reanalysis-I [*Menendez et al*., 2013]. Outputs provide hourly sea-state parameters (significant wave height, mean period, peak period, and mean wave direction) from 1948 to 2013.

Figure 2 shows the two selected study sites in the east of the North Atlantic basin: a location westward of Ireland (IR, lon = 11.25°W, lat = 53.25°N) and a site in the northwest coast of Spain (GA, lon = 9.25°W, lat = 43.5°N). GOW series of wave parameters in both sites have been compared against in situ observations in order to validate the data. Time series of hourly wave observations were obtained from the Irish Marine Buoy Network and the Spanish State Ports network. The Spanish 2246 buoy was moored in 1998 about 40 km west of A Coruña coast, at latitude 43.5°N and longitude 9.21°W. The Irish buoy M1 was deployed in 2000 about 95 km west of the Aran Islands, 53°07.6′N and 11°12.0′W. Figure 3 shows the validation process. The plots on the left show the scatterplot of buoy measurements and numerical results and the plots on the right show the buoy and GOW H_s hourly time series. Both tests demonstrate good agreement between the numerical data and observations, with a correlation higher than 0.9 and a low bias (0.014 and 0.354 m for the Spanish and Irish buoys, respectively). Buoy records can be used as input in the SD model. It should be noted, however, that long records and observations without gaps during specific seasons are recommended for a good statistical relationship between atmospheric patterns and local wave climate.

3.2. Predictor Definition

The wave climate along the European Atlantic coast is mainly influenced by extratropical storms generated in the north and northwest of the Atlantic basin with a mean duration and an arriving time to the east Atlantic coast of about 4 days [*Gulev et al*., 2001]. Figure 2 shows the area selected in the North Atlantic basin as the predictor spatial domain, from 25°N to 70°N and from 52.5°W to 10°E. The selected domain covers the storm activity in the North Atlantic Ocean which is the source of swell wave component on the northwest coast of Europe [*Alves*, 2006]. The predictor variables used in the statistical model are the SLP

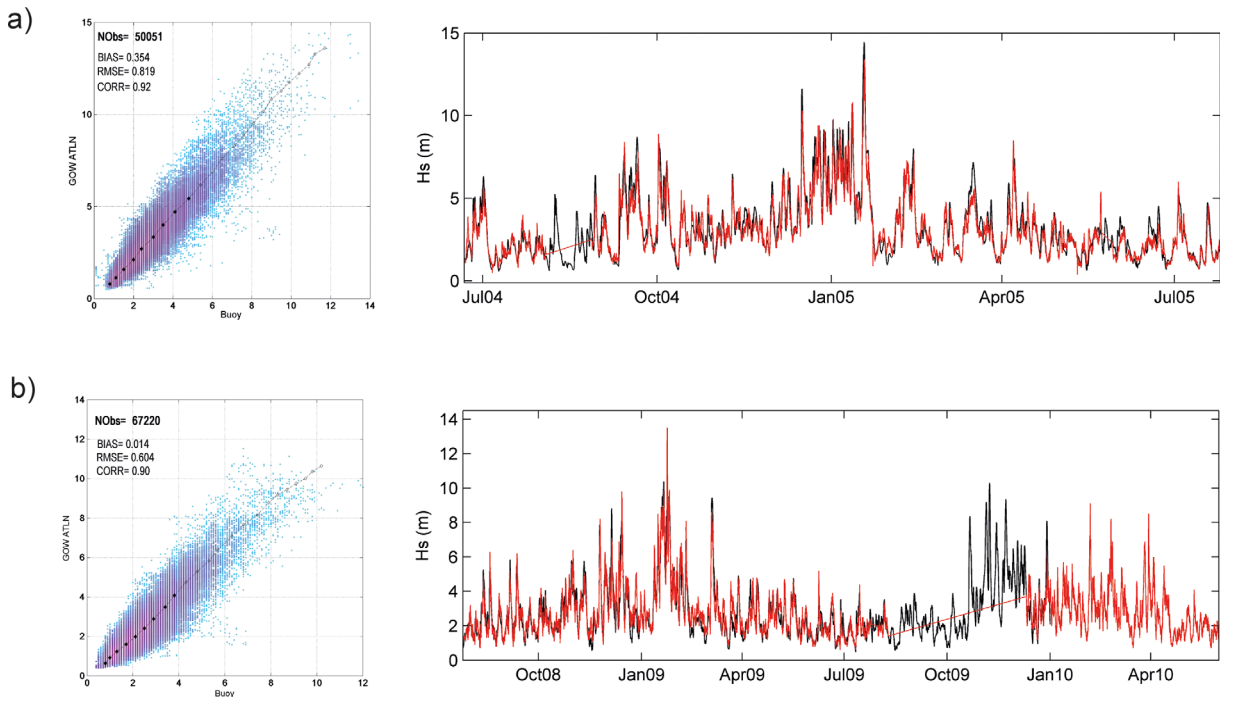

Figure 3. (left) Scatterplot and quantile-quantile plot and (right) time series of significant wave height (m) from buoy records versus GOW hindcast for a location in (a) west Ireland and (b) Norwest Spain. Buoy records are in red and GOW data in black.

fields and the squared SLP gradients (SLPG), which represent the geostrophic wind conditions. The land grid points of the selected domain are disregarded, avoiding the strong variability mode of SLPG over Greenland and other onshore regions. The predictor is defined as the three daily mean SLP and three daily mean SLPG, calculated every day through the calibration time period. Thus, the predictor associated with a certain day corresponds to the average obtained using the same day and the previous 2 days.

3.3. Statistical Downscaling Method

3.3.1. Weather Type Classification

First, the PCA analysis is applied to the SLP and SLPG daily data for the calibration period. In this example, the calibration period is a 40 year representative period from 1960 to 1999. In this study, a variance equal to 95% is considered, which corresponds to the first 38 PCs.

A number of $M = 100$ patterns is established in the application of KMA. The selection of a hundred classes is made based on the compromise between an easy handle characterization of synoptic climatologies and the best reproduction of monthly sea-state parameters (model validation). A sensitivity analysis of the model validation has been performed considering a different number of clusters, varying between $M = 20$ and $M = 400$. Figure 4 shows the 100 WTs, organized in a bidimensional lattice. In the figure, the WTs are represented by the isobars. The high-pressure systems over the averaged air pressure at sea level (1013 hPa) are displayed on a red scale and the low-pressure systems on a blue scale. Similar patterns are located together, varying smoothly from one cell to another. WTs with intense low-pressure systems but different locations of the pressure center are distributed at the corners of the lattice, being identified as different circulation patterns. The standard positive North Atlantic Oscillation (NAO) mode, characterized by a strengthening of the low over Iceland and the high around Azores islands, are at the bottom left corner of the lattice, while WTs with an intense low-pressure center on the North Atlantic Ocean between 40° and 58° latitudes are located at the bottom right corner of the lattice. These latter WTs can be associated with East Atlantic (EA) positive phase situations, a north-south dipole similar to NAO but with its center located southward (deeper low at 50°–55° and a higher subtropical high).

The seasonal or interannual variability can be analyzed using the WT classification. Figure 5 graphically shows the seasonal and total probability of the WTs from NCEP-NCAR reanalysis-I during the calibration

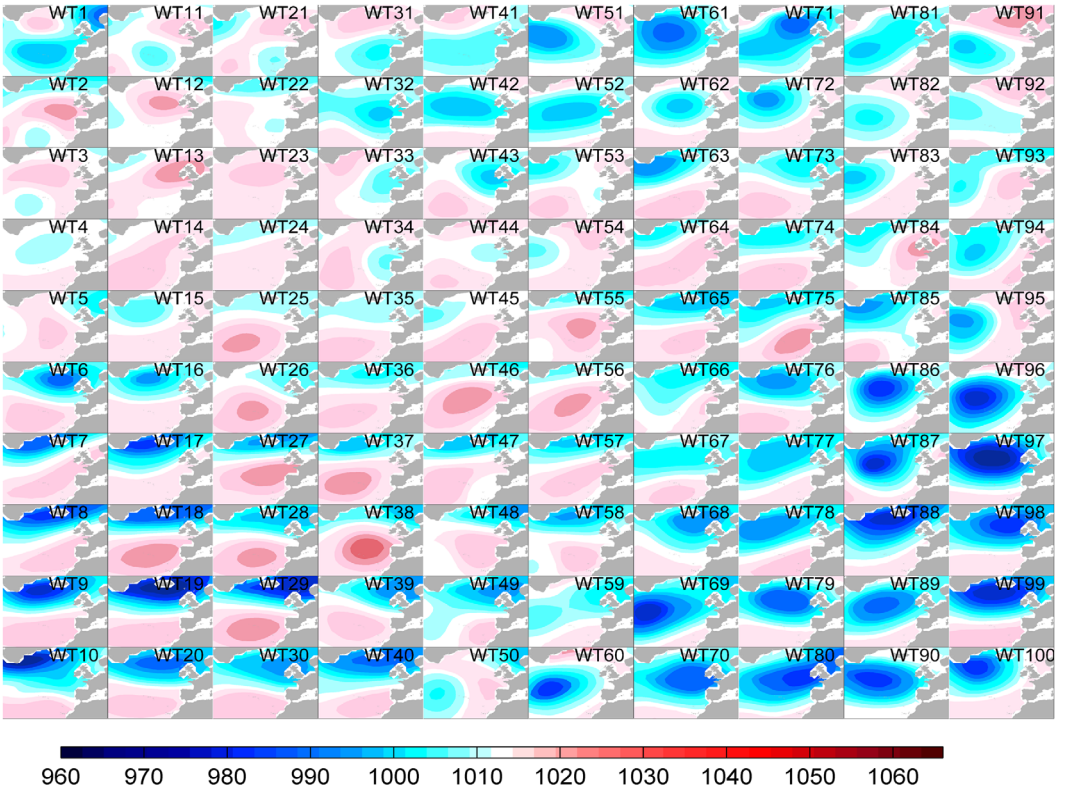

Figure 4. The 100 weather types represented by the SLP fields (hPa) obtained from the atmospheric classification.

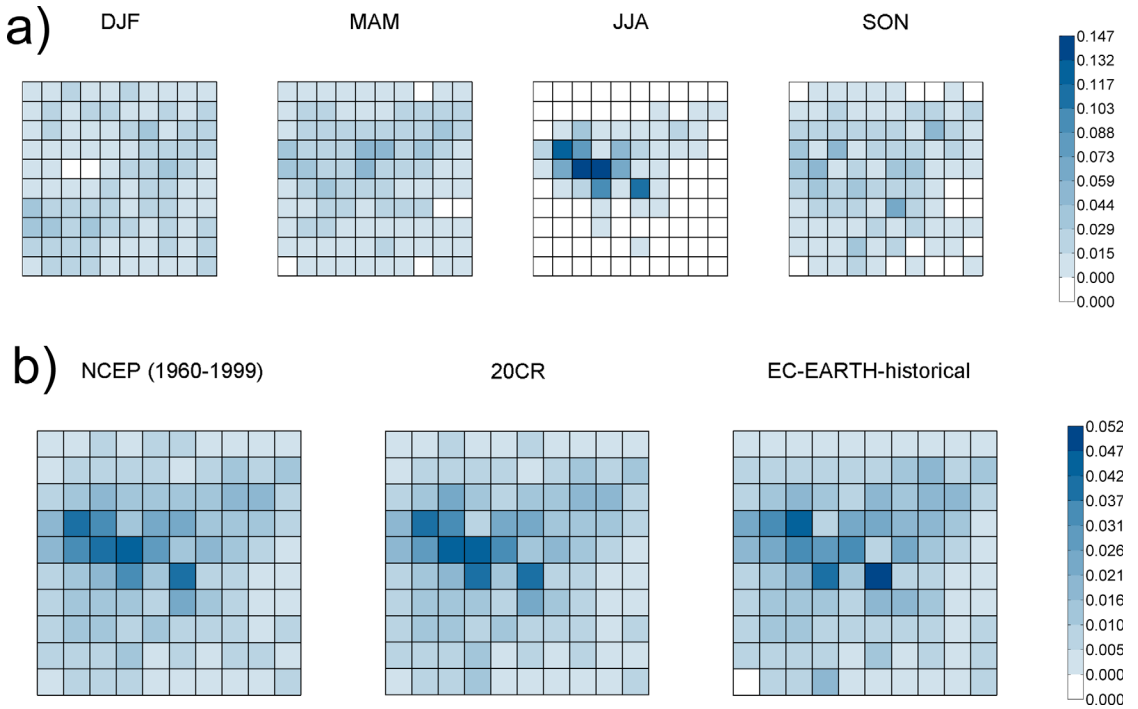

Figure 5. (a) Seasonal probability of occurrence of the 100 weather types (classification shown in Figure 4) for the NCEP-NCAR reanalysis-I for the calibration period 1960–1999. (b) Probability of occurrence for the present conditions (1960–1999) of the weather types from the NCEP-NCAR reanalysis-I, 20CR reanalysis, and climate model EC-EARTH, from left to right.

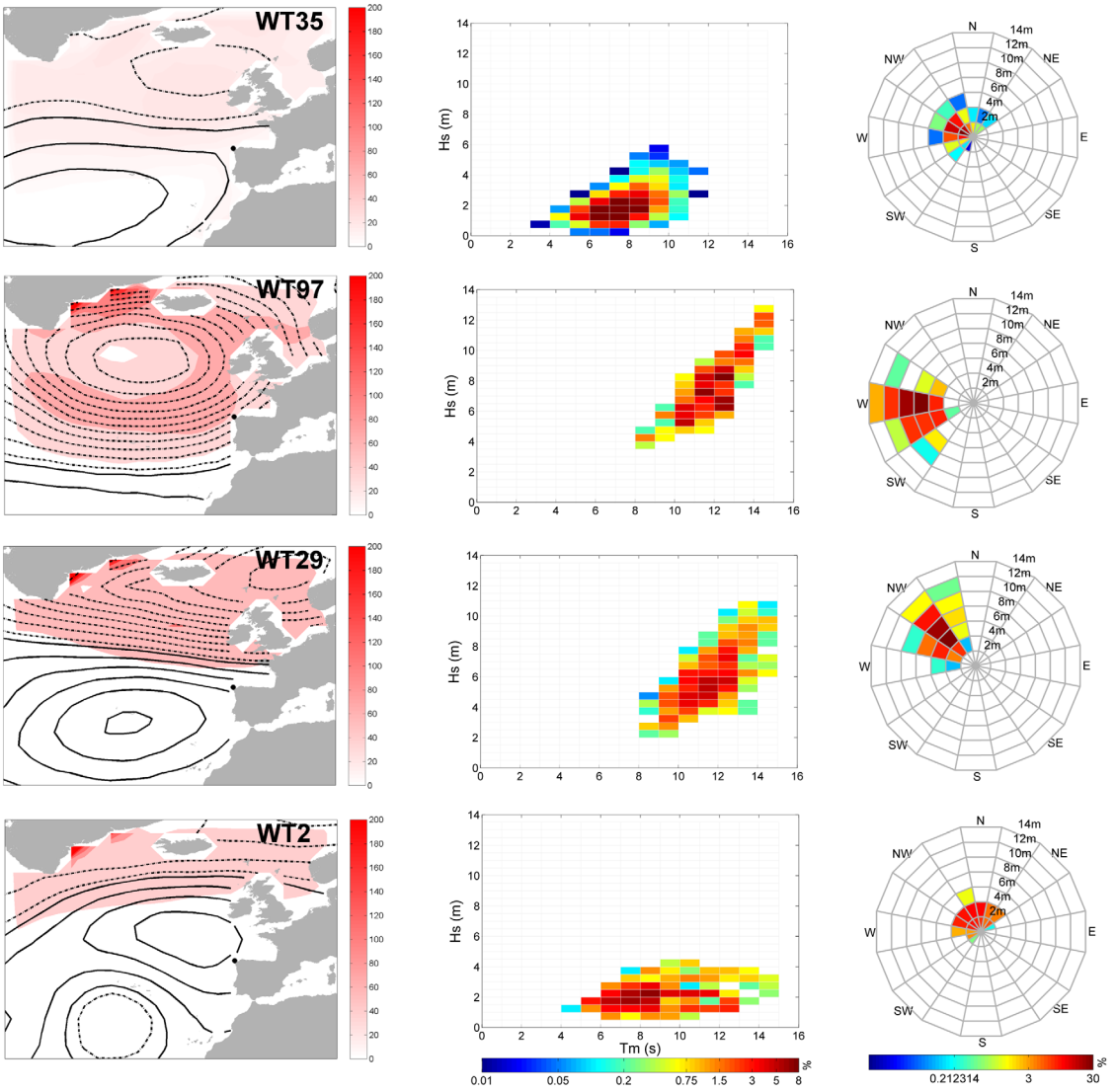

Figure 6. Several patterns (WT35, WT100, WT29, and WT2 from the WT classification shown in Figure 4) with the associated distribution of hourly significant wave height and mean period and distribution of the significant wave height and mean direction at GA location. The contours represent the SLP field (dashed below and continuous over 1013 hPa) and the red scale represents the SLPG.

period of 40 years. Darker blue color indicates WTs with high frequency and the lighter blue the most unusual. Winter season shows the largest variability of WTs while the synoptic patterns in summer are concentrated in several WTs located in the middle of the KMA lattice, corresponding to high-pressure situations. Patterns in the rest of seasons cover a wider range of WTs. The WTs in the corners of the lattice are detected only in winter (DJF), corresponding to a low-pressure center over the North Atlantic Ocean.

3.3.2. Relationship Between Predictor and Predictand

Besides being a description of atmospheric states, the classification is also a tool for understanding atmospheric processes and the linkage between circulation and surface climate [*Huth*, 2010]. In this section, the nonlinear relation between predictor (*X*, atmospheric conditions) and predictand (*Y*, local wave climate) is described.

The local wave climate data of the two selected locations are projected into the WT classification. The hourly sea-state parameters H_s, T_m, mean wave direction (θ_m), wave energy flux indicator ($H_s^2 T_m$), and the components *x* and *y* of the mean energy flux indicator, corresponding to daily predictor fields represented by each WT are projected in each pattern during the calibration period.

Figure 6 presents local wave climate information at the northwest Spanish location associated with four different WTs. The dominant WT in summer (WT35) represents a neutral atmospheric situation, with weak high

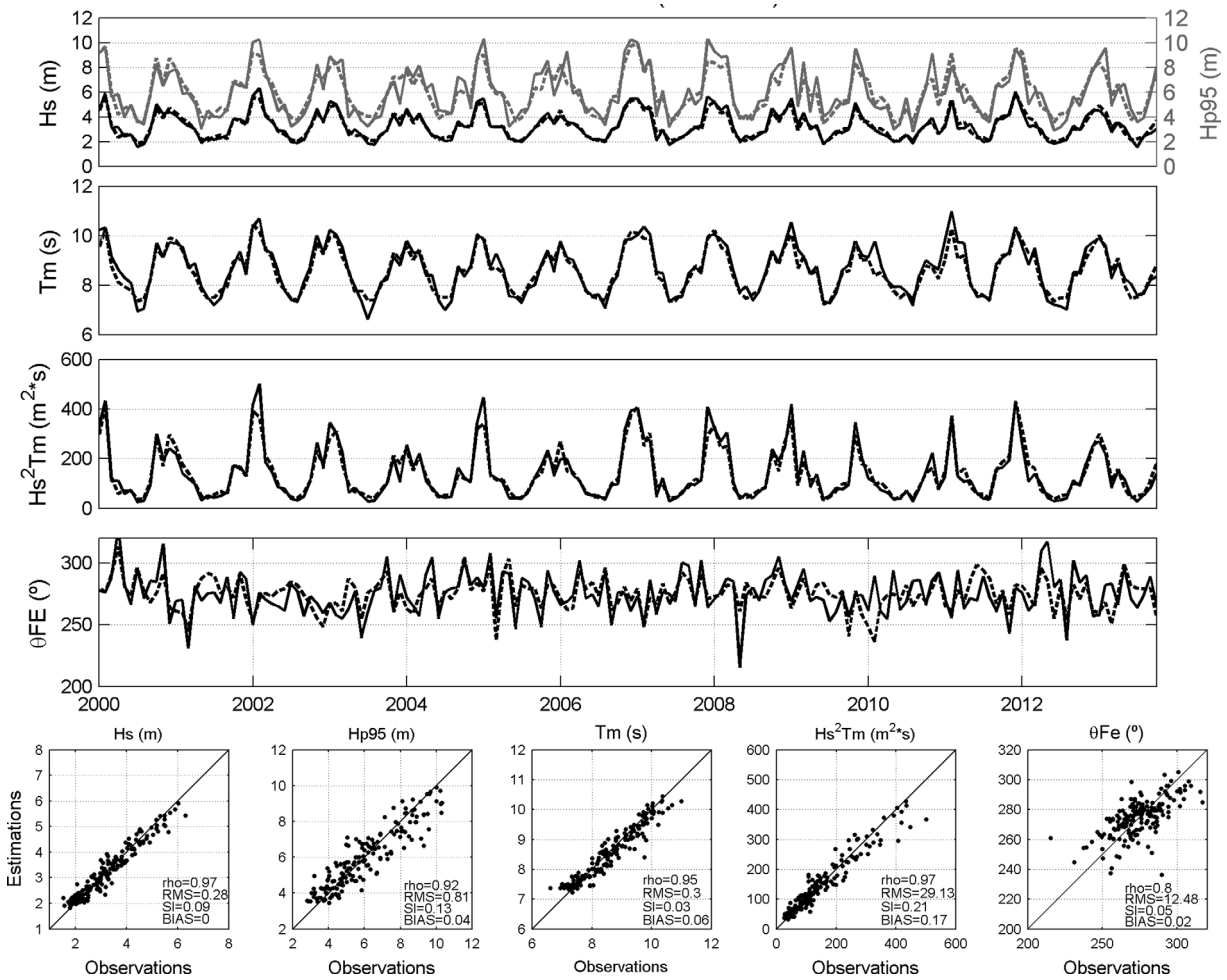

Figure 7. Time series comparison and scatterplots of the monthly sea-state parameters: H_s, H_{p95}, T_m, $H_s^2T_m$, θ_{FE} in the period 2001–2009 at the IR location. Solid lines show the GOW hindcast time series. Dashed lines represent the monthly parameters obtained from the downscaling framework proposed.

and low-pressure systems. The joint distribution $f_{35}(H_s,T_m)$ and the join distribution $f_{35}(H_s,\theta_m)$ are also displayed. The most probable H_s is around 1.5 m, the corresponding T_m is around 7 s, and θ_m is NW, although a wide range of directions from SW to NE are probable. WT97, a pattern that only occurs in winter, is also shown in Figure 6, with the associated joint distributions $f_{97}(H_s,T_m)$ and $f_{97}(H_s,\theta_m)$. In this case, WT97 represents an intense low-pressure system in the Northeast Atlantic with important SLPG. The atmospheric pattern is reflected in the associated sea states. H_s is around 9 m, T_m around 12 s, and θ_m mainly from W. H_s and T_m associated with WT35 and WT97 are clearly different, reflecting a predominant swell nature of waves in winter and local wind origin in summer. Other two patterns are also shown in Figure 6. WT29 is a winter pattern with a low-pressure center located northward which generates high energetic (lower H_s but larger T_m than WT97) northwesterly waves at GA location. WT2 represents a local high-pressure center with the associated sea waves mainly with a northeast direction at GA.

3.4. Validation of the Statistical Downscaling Method

In order to verify the skill of the SD method to predict multivariate wave climate, a validation analysis from 2000 to 2013 period is performed, comparing the estimations from the statistical downscaling model against the parameters obtained from the quasiobservations (GOW wave data).

The mean and 95 percentile of H_s (H_{p95}), T_m, $H_s^2T_m$, and mean wave energy flux direction (θ_{FE}) parameters are validated using the corresponding sea-state parameter distribution associated with each *WT* during the calibration period. Figures 7 and 8 show the comparison at the west Irish and northwest Spanish locations, respectively. The simulated monthly wave climate from the SD model is able to reproduce the quasi-real

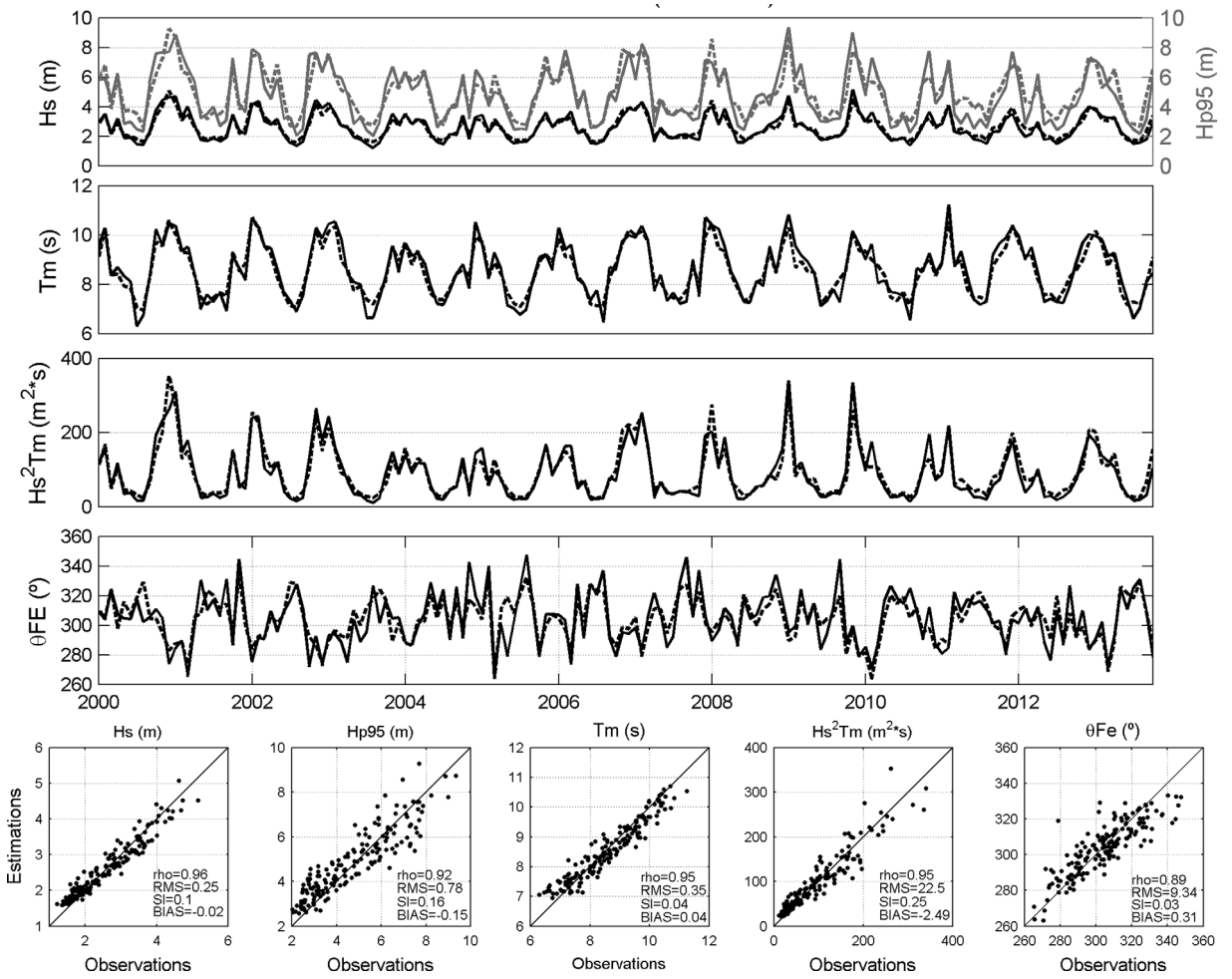

Figure 8. Time series comparison and scatterplots of the monthly sea-state parameters: H_s, H_p95, T_m, $H_s^2T_m$, θ_{FE} in the period 2001–2009 at the GA location. Solid lines show the GOW hindcast time series. Dashed lines represent the monthly parameters obtained from the downscaling framework proposed.

data, even for local maxima and minima monthly values of all the sea-state parameters analyzed. Although some discrepancies can be found for some specific months, the interannual variability of all these sea-state parameters is well reproduced for the two locations studied. The correlation coefficient (ρ), root mean square error (RMS), the scatter index (SI) and the bias are computed for each validated variable. It can be observed that the range of the correlation coefficient is between 0.80 and 0.97. The RMS is about 0.3 m for H_s, 0.3 s for T_m, 30 m^2 s for $H_s^2T_m$, and 11° for θ_{FE}. The largest differences are found for the 95 percentile of H_s (RMS = 0.81 at IR location and RMS = 0.78 at GA location) and θ_{FE} (RMS = 12.48 at IR location and RMS = 9.34 at GA location).

4. Applications of the Statistical Downscaling

A wave climate characterization to better understand the drivers of the local predictand is presented. Besides, this method also provides a useful tool to obtain local wave climate outside the calibration period. A wave hindcast for the whole twentieth century and for a short-term period (last winter) or wave climate projections are described.

4.1. Wave Climate Characterization

Besides obtaining the most representative synoptic situations in the NE Atlantic, the organized atmospheric classification provides the possibility of representing a local wave climate variable at a particular location on the 2-D lattice by projecting the variable value associated with each WT map. A connection between the

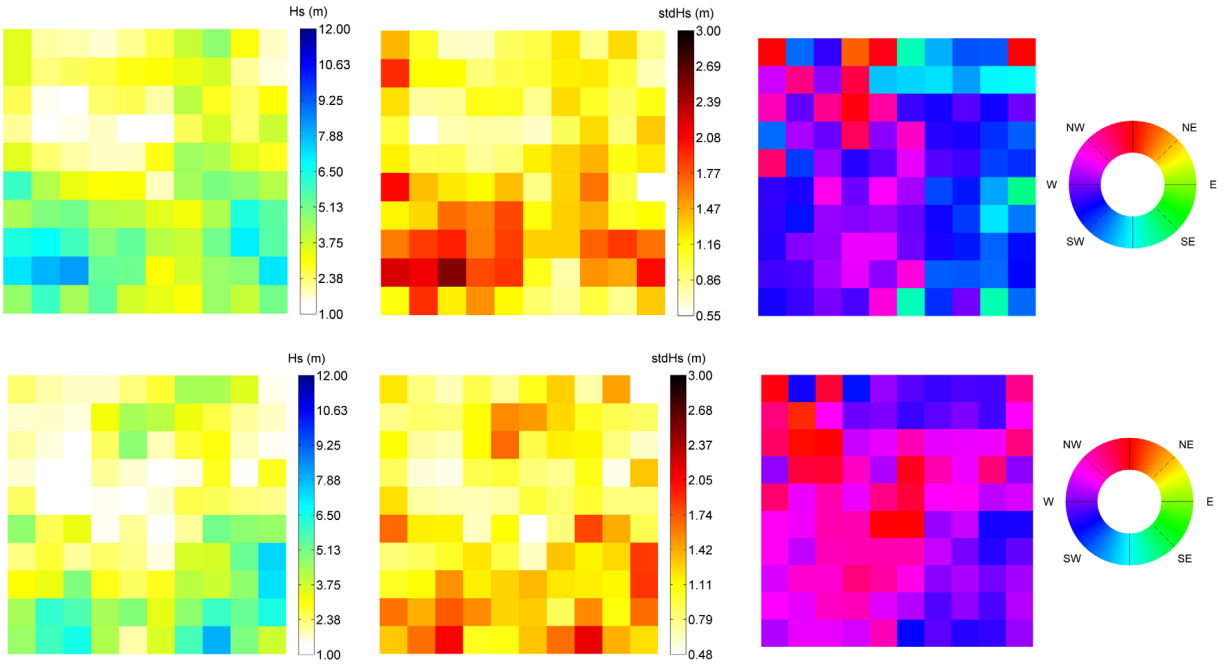

Figure 9. Wave climate characterization at the (top) west Irish location and (bottom) northwest Spanish location associated with WT classification (shown in Figure 4). (left) The mean significant wave height (units in m), (middle) standard deviation of the significant wave height (units in m), and (right) mean wave energy flux direction (units in °) associated with each WT.

circulation patterns on the North Atlantic Ocean and the wave climate in both locations is, therefore, established. Figure 9 shows the mean and standard deviation of H_s and θ_{FE} for each WT cluster at the IR and GA locations.

Larger mean significant wave heights, usually associated with high variances, are related to weather types with intense low-pressure centers at both bottom corners of the lattice. In the case of the Irish location, the patterns with larger waves correspond to positive NAO modes, with an intense low-pressure center around Iceland (left bottom WTs in the lattice). In the case of the Spanish location, the highest energetic waves can be associated with both, the standard positive NAO pattern and the positive EA pattern, showed in the WTs at the lower right corner of the lattice (i.e., the WT97 described previously as a specific winter pattern). EA WTs generate high energetic waves with a west-southwest mean direction, due to the fact that these spatial patterns are related with westerly winds, while NAO WTs are associated with slightly lower energetic waves with a northwest direction. The different wave conditions at both locations associated with these NAO and EA patterns reflect that a large fraction of wave anomalies in the North Atlantic Ocean, mainly in the northern part, is explained by NAO; while the high fraction of the rest of anomalies in the southern part is related to EA [*Woolf et al.*, 2002]. In the case of waves associated with the predominant summer patterns, located in the middle of the KMA lattice, a north mean energy flux direction reflects frequent high-pressure conditions that generate waves coming from north-northeast direction.

Figure 10 shows the bidimensional distribution of H_s and θ_m for the 100 WTs at the west Irish location. The WTs most clearly detected are the ones corresponding to the largest energetic sea states. As it is previously described, largest significant wave heights are associated with considerable low-pressure patterns, located at the corners of the KMA lattice. The location of the low-pressure center in the North Atlantic Ocean distinguishes the wave origin which it is mainly reflected in the wave direction. For example, northward low-pressure centers (positive NAO patterns) generate waves coming from the west at the Irish location and waves from the northwest at the Spanish location (e.g., WT19 or WT29). Higher periods associated with these WTs are also detected at the Spanish location due to a farther distance from the storm generation area (the associated distributions of H_s and T_m are not shown). Southward low-pressure centers (positive EA patterns) are linked to waves coming from the southwest at the Irish location or from the west at the Spanish location (e.g., WT87 or WT97). This southerly shift in wave direction is related to an EA positive pattern [*Charles et al.*, 2012]. Wave energy is more significant if the position of these centers is closer to the wave

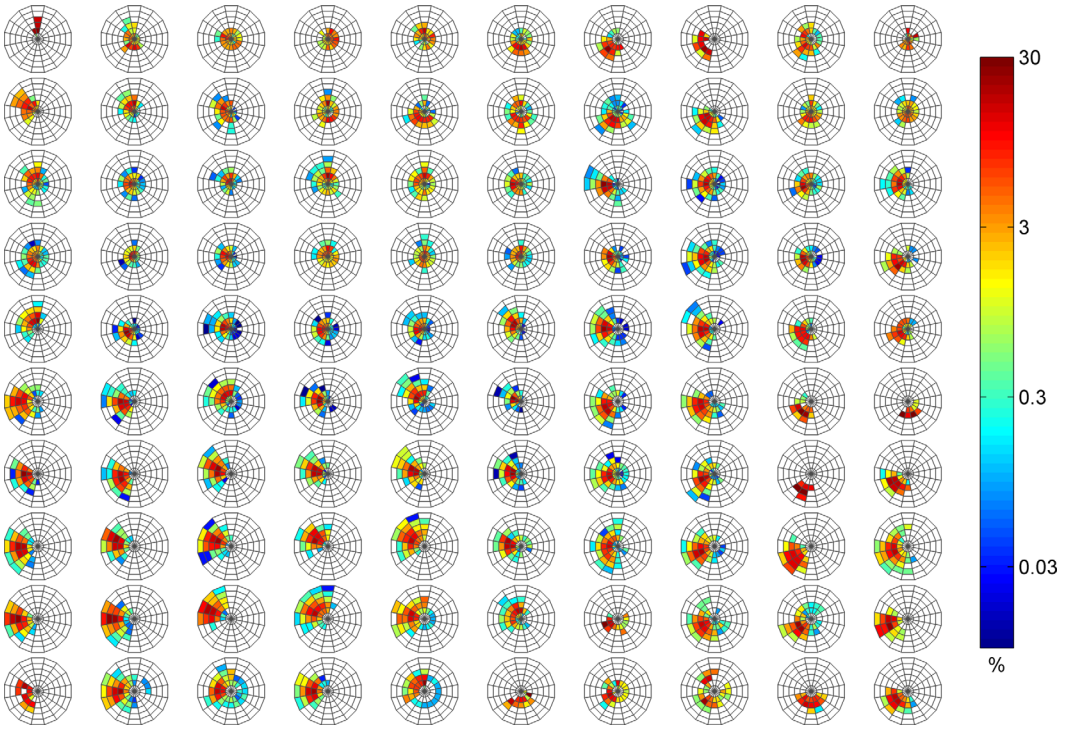

Figure 10. Distribution of the significant wave height and the mean wave direction associated with each weather type at the west Irish location (shown in Figure 4). The units of the radial distance are in m with the same scale as in Figure 6 (H_s increments are 2.0 m).

location (WT29 generates more energetic waves at Irish location, while WT97 generates more energetic waves at Spanish location). Neutral patterns are associated with low energetic waves coming (low values of H_s and T_m) from a wider range of directions, due to the fact that the predictor characterization of regional patterns while these waves are generated by local phenomena. Several WTs represent particular situations, e.g., WT1, is characterized by a high-pressure center at the latitude of the Irish location, which generates local waves from the north at this location. These differences in the wave direction are detected in the wave climate characterization by means of the mean value of the significant wave height and mean energy flux direction associated with each WT.

4.2. Wave Climate Hindcast

A long-term wave climate historical reconstruction and a short-term wave hindcast in winter 2013–2014 require historical or forecasted information of the synoptic circulation systems.

The local long-term wave climate historical reconstruction is derived from the twentieth century atmospheric reanalysis SLP data (20CR) [*Compo et al*., 2011]. The 20CR is a global reanalysis spanning the twentieth century, created by the NOAA ESRL/PSD. The SLP fields are available at 6 hourly temporal and 2° horizontal resolution. In this reanalysis, pressure observations have been combined with a short-term forecast ensemble of an NCEP numerical weather prediction model. The use of the SLP fields from 20CR as a historical predictor into the SD model is validated by assessing the occurrence rates of the hundred WTs during the calibration period against the NCEP-NCAR reanalysis-I (Figure 5b). Once the pressure data source is considered suitable, the probability of occurrence of the WTs throughout the XX century is estimated to reconstruct the historical wave climate.

Figure 11a shows the monthly mean reconstructed H_s at the two study sites since 1900. Figure 11b shows the comparison of winter H_s (DJFM) between the statistically downscaled 20CR (black) and the SD NCEP reanalysis-I (blue). This comparison reveals a good agreement between the wave hindcasts and a high skill to simulate the climate variability. The GA location (2.63 m mean H_s and 3.44 m winter mean H_s for 1900–2010) does not present such high wave climatologies as IR location (3.24 and 4.24 m, respectively). An interesting point is that, while GA location shows homogeneous interannual variations with maxima along the

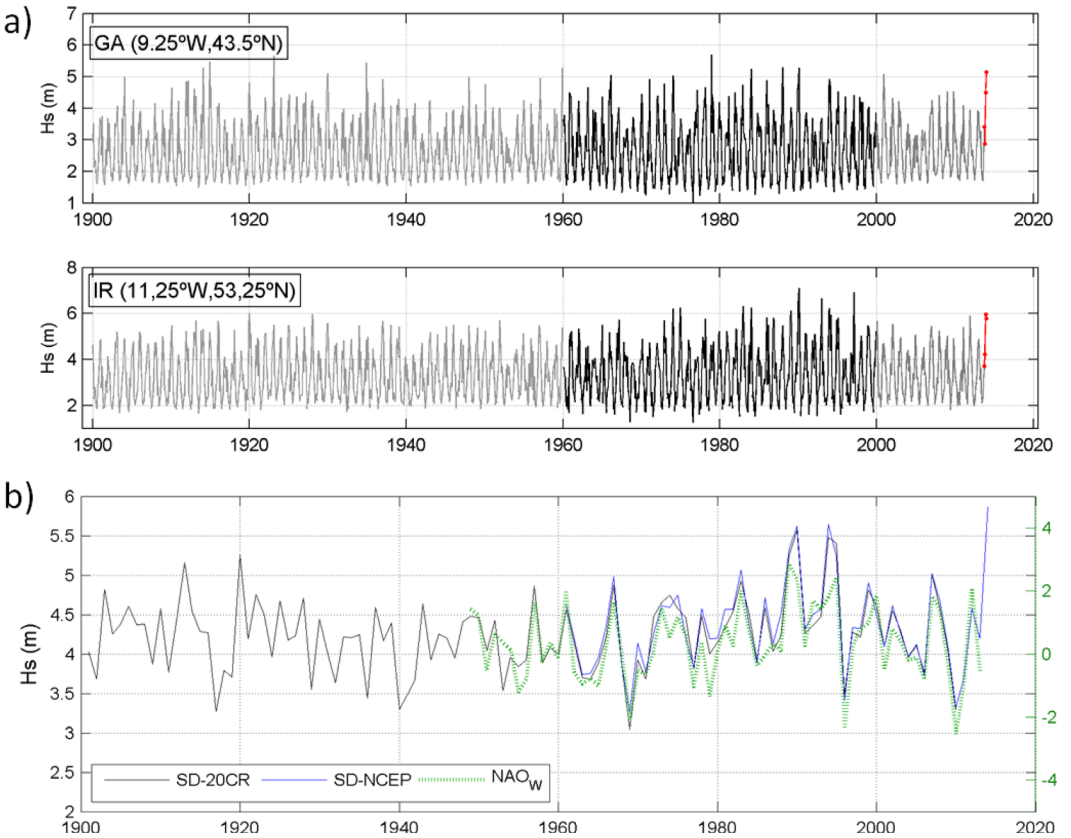

Figure 11. (a) Time series of the monthly H_s historical reconstruction from 20CR (1900–1960), NCEP-NCAR reanalysis-I for the calibration period (1960–2000) and the validation period (2001–2013) and the winter 2013–2014 (red line) for the two target points. (b) Winter H_s (DJFM) reconstruction from 20CR (black) and NCEP-NCAR reanalysis-I (blue) at IR location and the NAO winter climate index (green).

whole period, IR largest values are observed during the period 1970–2000. Several studies have already accomplished a wave climate reconstruction from 20CR on North Atlantic. *Bertin et al*. [2013] developed a dynamic downscaling with the numerical model WaveWatch III forced with wind and ice fields from 20CR. *Wang et al*. [2012] obtained reconstructed waves by a regression SD model using 20CR SLP as predictor. For comparison, the mean and linear trends of H_s from the proposed SD approach during several periods were assessed. We have found that our mean H_s at the two target locations are similar to those from *Bertin et al*. [2013] for the period 1900–2008 (3.2 m at IR and 2.6 m at GA) but differ from those of *Wang et al*. [2012] for the period 1958–2001 (2.9 m at IR and 2.4 m at GA). Lower estimates are obtained from the SD model of *Wang et al*. [2012], nevertheless our mean H_s are similar to the dynamically downscaled waves from MSC50 [*Cox and Swail*, 2001] for the same period (3.2 m at IR and 2.6 m at GA). On the other hand, the analysis of the H_s linear trends reveals an increase for 1958–2001 (0.5 and 0.15 cm/yr at IR and GA locations, respectively) similar to those found by the SD model by *Wang et al*. [2012], 0.45 cm/yr at IR and 0.10 cm/yr at GA, and the MSC50 data (0.50 cm/yr at IR and 0.10 cm/yr at GA), but our estimated trend at IR location (0.019 cm/yr) for the XX century differs from *Bertin et al*. [2013], who found higher positive trends on the Northeast Atlantic (0.6 cm/yr at IR). It is noteworthy that after the period 1958–2000 with an increase in wave intensity, estimated trends over the last 30 years (1980–2009) are significantly negative at the two studied points for both, mean and winter H_s (-0.23 cm/yr mean H_s trend and -1.78 cm/yr winter H_s trend at IR location and $-0.17/-0.96$ cm/yr, respectively, at the GA location). In order to better understand these trends, the multidecadal and interannual wave variability driven by the NAO [*Woolf et al*., 2002] was analyzed. According to *Bertin et al*. [2013], we have found a large positive correlation with winter NAO [*Jones et al*., 1997] at the IR point in the NE Atlantic (0.64 Pearson correlation, Figure 11b) and a weak positive correlation at the GA location in South-East Atlantic (0.035 Pearson correlation). The stronger relation between NAO and waves at IR location explains the multidecadal wave climate variability. A decrease of wave height coincides with a decline of the NAO to the 1960s, an increase of wave height in the period 1958–2000 with

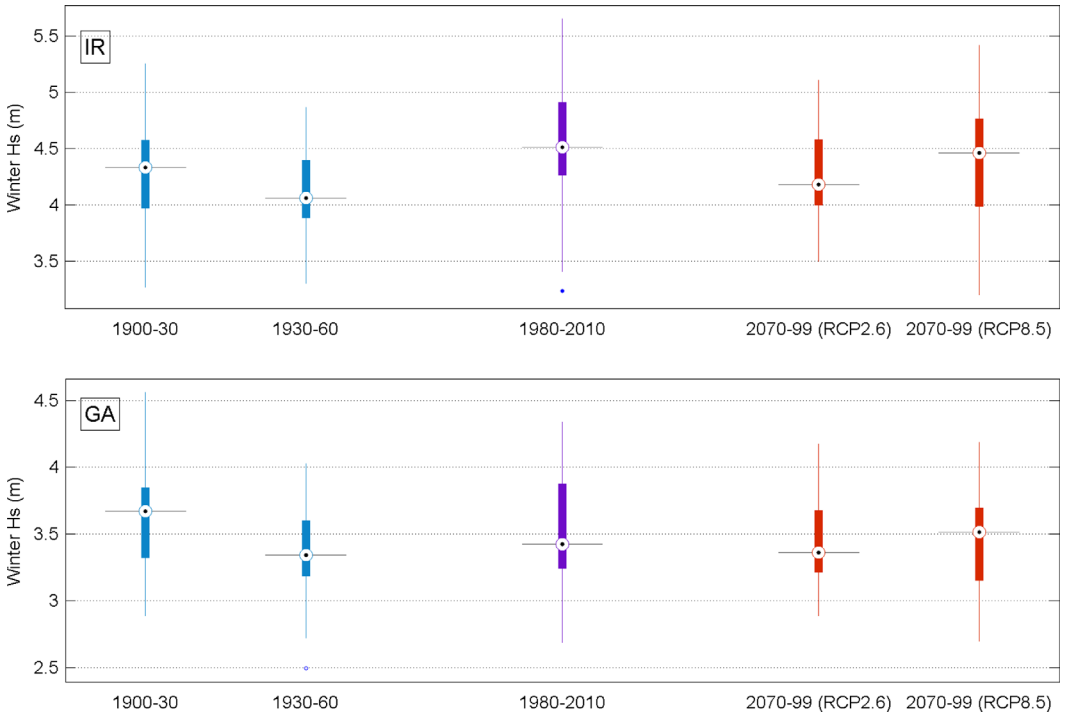

Figure 12. Box plots of H_s winter (DJFM) for present climatology (1980–2010), historical reconstructed periods (1900–1930, 1930–1960), and future projected climate scenarios (2070–2100) for the EC-Earth model. On each box, the central mark is the median, the edges of the box are the lower (Q1) and upper (Q3) quartiles (interquartile range, IQR), and the whiskers extend to the higher values, within the range defined by Q1 − 1.5(IQR) and Q3 + 1.5(IQR).

the NAO rise to early 1990s. Therefore, the decrease in the last 30 years could be influenced by the recent smaller NAO fall.

The SD method provides a tool to update wave climate information of numerical outcomes with low computational cost. Here, we have hindcasted the winter 2013–2014, a particularly large winter with a strong jet stream driving across the Atlantic and causing large wave storms affecting Portugal and Spain. Red lines in Figure 11 indicate the estimated monthly mean H_s. The larger waves which arrive to the European coast in winter 2013–2014 are shown, reaching 5 m, at GA location and 6 m at IR location. We note that the SD model can also be used as a forecast tool in a similar way.

4.3. Wave Climate Projections

The future projections of local waves from the outputs of a GCM under different climate change scenarios can be obtained applying the SD model. We use the EC-Earth GCM [*Hazeleger et al*., 2012], from a European consortium with collaborations of 27 Institutions. EC-Earth model is formed by the Integrated Forecast System (IFS) of the European Centre for Medium Range Weather Forecasts (ECMWF). Here we use the SLP data of the CMIP5 experiments, called historical for recent past conditions and RCPs (Representative Concentration Pathways) [*Moss et al*., 2010] for the future runs. The selected RCPs included one mitigation scenario leading to a very low forcing level (RCP2.6) and one very high baseline emission scenario (RCP8.5), leading to high greenhouse concentration levels. *Perez et al*. [2014] analyzed numerous CMIP3 and CMIP5 GCMs and found that EC-Earth is one of the most skilled in the North Atlantic region. Moreover, the EC-Earth model is able to reproduce the occurrence of the synoptic atmospheric conditions during the historical period (Figure 5b).

Figure 12 shows the resulting box plots of the estimated winter H_s of the SD model for historical, present, and projected 30 year periods at the two studied locations. A slight decrease on future winter H_s relative to the present climate time slice is detected, being winter H_s from RCP8.5 higher than RCP2.6. Ensemble CMIP5-based statistical wave projections also provide a general decrease of annual H_s in the midlatitudes of the North Atlantic for the period 2080–2099 relative to the period 1980–1999 for the RCP8.5 scenario [*Wang*

et al., 2014]. It is interesting to point out the projected values in 2070–2099 at GA and IR locations do not show variations on mean and variance different to those reconstructed in the past.

5. Summary and Conclusions

A statistical downscaling framework to project wave climate is proposed based on weather typing. The statistical relation is established between the atmospheric predictor, defined by the SLP fields and the squared SLP gradients, and the local wave climate. The model is applied in two locations on the Atlantic coast of Europe: west Ireland and northwest Spain. Waves in these two locations are generated by storms in the North Atlantic. Therefore, the spatial domain of the predictor is defined taking into account the storm activity in this area. Three days are considered as the mean period representative of the recent atmospheric conditions responsible for waves arriving at the studied locations. Three days mean predictor fields are calculated on a day-to-day basis, associated with the last day. PCA is applied to this daily predictor to reduce the data dimensionality and simplify the application of the classification technique. Weather types are obtained using KMA technique, with a postorganization onto a bidimensional lattice by a similarity criterion. The distribution of hourly sea states associated with each weather pattern is statistically established.

The method has been validated and several applications are shown. The following features of the proposed method are relevant: (1) The SD method is able to integrate different time and spatial scales of the wave generation and propagation processes. Statistical relationships between predictor and predictand are solved integrating 3 days history in the daily predictor over the generation area using WT approach. (2) The weather typing approach provides a physical explanation of the relation between local waves and regional synoptic atmospheric conditions. The application of the SD model at two locations northward and southward East Atlantic Ocean reveals clear associations with specific low/high-pressure systems in the Atlantic Ocean. (3) The SD method provides multivariate results of wave climate. Univariate or bivariate empirical probability density functions of different sea-state parameters are estimated using this SD method. Other statistics, besides the mean value, can be predicted. Further research is needed to extend this approach to statistically model extreme values conditioned to a particular WT, following for instance the method proposed by *Izaguirre et al*. [2012].

The applied SD model provides these conclusions:

1. The local multivariate wave climate can be characterized based on a physical relation with atmospheric conditions.
2. The model validation proves to reproduce the seasonal and interannual variability of the monthly mean and 95 percentile of H_s, T_m, $H_s^2 T_m$, and θ_{FE}. Therefore, the proposed SD method is a useful tool for coastal impact assessment.
3. The SD model is able to produce long historical reconstructions. SLP forcing from 20CR reanalysis is used to reconstruct local waves through the XX century, obtaining wave statistics and trends in agreement with previous works by other authors [*Bertin et al*., 2013; *Wang et al*., 2012]. Moreover, the obtained results are similar to those obtained by dynamical downscaling techniques [*Bertin et al*., 2013; *Cox and Swail*, 2001] that take into account the complex processes of wave generation, propagation, and dissipation numerically. The advantage of the SD method is the low computational time to characterize wave climate without information of wind fields and bathymetry.
4. The update of the local wave hindcast in the last winter shows the applicability of the SD approach for seasonal forecast.
5. The SD model is a useful tool to get wave climate multimodel ensemble projections with low computational cost. A negative trend has been detected for the end of this century, in accordance with *Wang et al*. [2014]. Nevertheless, the detected decrease is similar to modeled historical variations in the XX century.
6. Regarding future projections, we should note the limitations of the SD model from the implied assumptions of the statistical approach: A stationary statistical relationship and projected changes should lie within the range of the natural variability. SD model is unable to generate local waves from exceptional weather conditions that are not registered in the past.
7. The application of this statistical method to downscale wave climate at different locations around the globe required to adapt the predictor spatial domain to the area of influence of the wave energy

reaching the particular location of interest. Besides, the number of days to calculate the mean predictor fields needs to reflect the time wave energy takes to reach that particular location, strongly related to the storminess over the ocean basin.

Acknowledgments

The work was partly funded by the project iMar21 (CTM2010-15009) from the Spanish Government and the FP7 European projects CoCoNet (287844) and Mermaid (288710). The authors thank Puertos del Estado (Spanish Ministry of Public Works) and the Irish Marine Institute for providing the gauge records. Instrumental wave data could be requested from the archives of the Marine Institute at https://www.marine.ie/home/publicationsdata/RequestForData.htm, in the case of the Irish buoy, and from the repository of the Puertos del Estado at http://www.puertos.es/oceanografia_y_meteorologia/faqs.html, in the case of the Spanish buoy. Wave data from Global Ocean Waves (GOW) database could be requested to Environmental Hydraulics Institute at email address: ihdata@ihcantabria.com. NCEP reanalysis data are provided by the NOAA/OAR/ESRL PSD, Boulder, Colorado, USA, from their Web site at http://www.esrl.noaa.gov/psd/. NOAA CIRES Twentieth Century Global Reanalysis Version 2 is available at Research Data Archive at the National Center for Atmospheric Research, Computational and Information Systems Laboratory, http://dx.doi.org/10.5065/D6QR4V37. EC-EARTH data are available through the Earth System Grid-Center for Enabling Technologies (ESG-CET), on the page http://pcmdi9.llnl.gov/.

References

Alves, J.-H. G. M. (2006), Numerical modeling of ocean swell contributions to the global wind-wave climate, *Ocean Modell.*, *11*, 98–122.

Bermejo, M., and R. Ancell (2009), Observed changes in extreme temperatures over Spain during 1957–2002, using Weather Types, *Rev. Climatol.*, *9*, 45–61.

Bertin, X., E. Prouteau, and C. Letetrel (2013), A significant increase in wave height in the North Atlantic Ocean over the 20th century, *Global Planet. Change*, *106*, 77–83.

Caires, S., V. L. Swail, and X. L. Wang (2006), Projection and analysis of extreme wave climate, *J. Clim.*, *19*, 5581–5605.

Camus, P., F. J. Méndez, R. Medina, and A. S. Cofiño (2011), Analysis of clustering and selection algorithms for the study of multivariate wave climate, *Coastal Eng.*, *58*(6), 453–462.

Casas-Prat, M., X. L. Wang, and J. P. Sierra (2014), A physical-based statistical method for modeling ocean wave heights, *Ocean Modell.*, *73*, 59–75.

Charles, E., D. Idier, J. Thièbot, G. Le Cozannet, and R. Pedreros (2012), Present wave climate in the Bay of Biscay: Spatiotemporal variability and trends from 1958 to 2001, *J. Clim.*, *25*, 2020–2039.

Compo, G. P., et al. (2011), The twentieth century reanalysis project, *Q. J. R. Meteorol. Soc.*, *137*, 1–28, doi:10.1002/qj.776.

Cox, A. T., and V. R. Swail (2001), A global wave hindcast over the period 1958–1997: Validation and climate assessment, *J. Geophys. Res.*, *106*(C2), 2313–2329.

Fowler, H. J., S. Blenkinsop, and C. Tebaldi (2007), Linking climate change modelling to impact studies: Recent advances in downscaling techniques for hydrological modelling, *Int. J. Climatol.*, *27*, 1547–1578.

Giorgi, F., B. Hewitson, J. Christensen, M. Hulme, H. von Storch, P. Whetton, R. Jones, L. Mearns, and C. Fu (2001), Regional climate information—Evaluation and projections, in *Climate Change 2001. The Scientific Basis. Contribution of Working Group to the Third Assessment Report of the IPCC: Contribution to Working Group I*, edited by J. T. Houghton et al., chap. 10, pp. 583–638, Cambridge Univ. Press, Cambridge, U. K.

Gulev, S. K., and V. Grigorieva (2006), Variability of the winter wind waves and swell in the North Atlantic and North Pacific as revealed by the voluntary observing ship data, *J. Clim.*, *19*, 5667–5685.

Gulev, S. K., O. Zolina, and S. Grigoriev (2001), Extratropical cyclone variability in the Northern Hemisphere winter from the NCEP/NCAR reanalysis data, *Clim. Dyn.*, *17*, 795–809.

Gulev, S. K., V. Grigorieva, A. Sterl, and D. Woolf (2003), Assessment of the reliability of wave observations from voluntary observing ships: Insights from the validation of a global wind wave climatology based on voluntary observing ship data, *J. Geophys. Res.*, *108*(C7), 3236, doi:10.1029/2002JC001437.

Gutiérrez, J. M., D. San-Martín, S. Brands, R. Manzanas, and S. Herrera (2013), Reassessing statistical downscaling techniques for their robust application under climate change conditions, *J. Clim.*, *26*(1), 171–188.

Hastie, T., R. Tibshirani, and J. Friedman (2001), *The Elements of Statistical Learning*, Springer, N. Y.

Hazeleger, W., et al. (2012), EC-Earth V2.2: Description and validation of a new seamless earth system prediction model, *Clim. Dyn.*, *39*(11), 2611–2629.

Hemer, M. A., X. L. Wang, J. A. Church, and V. R. Swail (2010), Coordinating global ocean wave climate projections, *Bull. Am. Meteorol. Soc.*, *91*(4), 451–454.

Hemer, M. A., X. L. Wang, R. Weisssse, and V. R. Swail (2012), Advancing wind-waves climate science: The COWCLIP project, *Bull. Am. Meteorol. Soc.*, *93*(6), 791–796.

Huth, R. (2010), Synoptic-climatological applicability of circulation classifications from the COST733 collection: First results, *Phys. Chem. Earth*, *35*(9–12), 388–394.

Izaguirre, C., F. J. Méndez, M. Menéndez, A. Luceño, and I. J. Losada (2010), Extreme wave climate variability in southern Europe using satellite data, *J. Geophys. Res.*, *115*, C04009, doi:10.1029/2009JC005802.

Izaguirre, C., M. Menéndez, P. Camus, F. J. Méndez, R. Mínguez, and I. J. Losada (2012), Exploring the interannual variability of extreme wave climate in the Northeast Atlantic Ocean, *Ocean Modell.*, *59–60*, 31–40.

Izaguirre, C., F. J. Méndez, A. Espejo, I. J. Losada, and B. G. Reguero (2013), Extreme wave climate changes in Central-South America, *Clim. Change*, *119*, 277–290.

Jones, P. D., T. Jonsson, and D. Wheeler (1997), Extension to the North Atlantic Oscillation using early instrumental pressure observations from Gibraltar and South-West Iceland, *Int. J. Climatol.*, *17*, 1433–1450.

Kalnay, E., et al. (1996), The NCEP/NCAR 40-year reanalysis project, *Bull. Am. Meteorol. Soc.*, *77*, 437–470.

Kistler, R., et al. (2001), The NCEP–NCAR 50-year reanalysis: Monthly means CD-ROM and documentation, *Bull. Am. Meteorol. Soc.*, *82*, 247–267.

Maraun, D., et al. (2010), Precipitation downscaling under climate change: Recent developments to bridge the gap between dynamical models and the end user, *Rev. Geophys.*, *48*, RG3003, doi:10.1029/2009RG000314.

Menendez, M., M. García-Díez, L. Fita, J. Fernández, F. J. Méndez, and J. M. Gutiérrez (2013), High-resolution sea wind hindcasts over the Mediterranean area, *Clim. Dyn.*, *42*, 1857–1872, doi:10.1007/s00382-013-1912-8.

Moss, R. H., J. A. Edmonds, K. A. Hibbard, M. R. Manning, S. K. Rose, D. P. van Vuuren, T. R. Carter, S. Emori, M. Kainuma, and T. Kram (2010), The next generation of scenarios for climate change research and assessment, *Nature*, *463*, 747–756.

Perez, J., M. Menendez, F. J. Mendez, and I. J. Losada (2014), Evaluating the performance of CMIP3 and CMIP5 global climate models over the north-east Atlantic region, *Clim. Dyn.*, doi:10.1007/s00382-014-2078-8, in press.

Reguero, B. G., M. Menéndez, F. J. Méndez, R. Mínguez, and I. J. Losada (2012), A global ocean wave (GOW) calibrated reanalysis from 1948 onwards, *Coastal Eng.*, *65*, 38–55.

Sterl, A. (2004), On the (in)homogeneity of reanalysis products, *J. Clim.*, *17*, 3866–3873.

Suh, K., S. Kim, N. Mori, and H. Mase (2012), Effect of climate change on performance-based design of Caisson Breakwaters, *J. Waterw. Port Coastal Ocean Eng.*, *138*(3), 215–225.

Tolman, H. L. (2009), User manual and system documentation of Wavewatch-III version 3.14, *NOAA/NWS/NCEP Tech. Note 276*, 194, Camp Springs, Md.

Wang, X. L., and V. R. Swail (2006), Climate change signal and uncertainty in projections of ocean wave heights, *Clim. Dyn.*, *26*, 109–126.
Wang, X. L., F. W. Zwiers, and V. R. Swail (2004), North Atlantic Ocean wave climate change scenarios for the twenty-first century, *J. Clim.*, *17*, 2368–2383.
Wang, X. L., Y. Feng, and V. R. Swail (2012), North Atlantic wave height trends as reconstructed from the 20th century reanalysis, *Geophys. Res. Lett.*, *39*, L18705, doi:10.1029/2012GL053381.
Wang, X. L., Y. Feng, and V. R. Swail (2014), Changes in global ocean wave heights as projected using multimodel CMIP5 simulations, *Geophys. Res. Lett.*, *41*, 1026–1034, doi:10.1002/2013GL058650.
Wilby, R. L., S. P. Charles, E. Zorita, B. Timbal, P. Whetton, and L. O. Mearns (2004), Guidelines for use of climate scenarios developed from statistical downscaling methods, IPCC Task Group on Data and Scenario Support for Impact and Climate Analysis (TGICA). [Available at http://www.ipcc-data.org/guidelines/dgm_no2_v1_09_2004.pdf.]
Woolf, D. K., P. G. Challenor, and P. D. Cotton (2002), Variability and predictability of the North Atlantic wave climate, *J. Geophys. Res.*, *107*(C10), 3145, doi:10.1029/2001JC001124.